

# Predicting Electron Transport Using Simulated Axial Waves in a Radial-Axial Hybrid Hall Thruster Model

IEPC-2009-129

*Presented at the 31st International Electric Propulsion Conference,  
University of Michigan • Ann Arbor, Michigan • USA  
September 20 – 24, 2009*

Michelle K. Scharfe<sup>1</sup>  
ERC Inc., Edwards AFB, CA, 93524, USA

Mark A. Cappelli<sup>2</sup>  
Stanford University, Stanford, CA, 94305, USA

and

Eduardo Fernandez<sup>3</sup>  
Eckerd College, St. Petersburg, FL, 33711, USA

Axial waves predicted by a two-dimensional hybrid numerical model have been used to estimate electron cross field transport due to tilted waves with azimuthal components. Since the radial-axial hybrid simulation cannot model these tilted waves directly, the predicted axial waves are assumed to couple symmetrically into two counter-propagating axial-azimuthal waves. A linearized two-dimensional dispersion relation is solved to obtain the azimuthal component of wavenumber consistent with the frequency and axial wavenumbers predicted by the radial-axial simulation. The resulting transport profiles are in qualitative agreement with experimental measurements of electron mobility when the power levels of the fluctuations approach saturation levels. For large amplitude fluctuations, the predicted electron mobility profile exhibits a transport barrier near the exit plane of the thruster consistent with experimental measurements, suggesting that this barrier may be due to a transition from transport-enhancing azimuthal waves to transport-limiting axial waves in this region.

## Nomenclature

$\vec{B}$	= magnetic field, T
$\vec{E}$	= electric field, V/m
$\vec{J}$	= current density, A/m <sup>2</sup>
$T$	= temperature, K
$\vec{U}$	= velocity, m/s
$e$	= electron charge, C
$f$	= arbitrary fluctuating quantity
$k_b$	= Boltzmann constant, J/K

---

<sup>1</sup> Staff Scientist, AFRL/RZSS, michelle.scharfe.ctr@edwards.af.mil

<sup>2</sup> Professor, Mechanical Engineering Department, cap@stanford.edu

<sup>3</sup> Associate Professor, Mathematics and Physics Department, fernane@eckerd.edu

$\bar{k}$	= perturbation wavenumber, 1/m
$m$	= mass, kg
$n$	= number density, 1/m <sup>3</sup>
$p$	= pressure, N/m <sup>2</sup>
$q$	= charge, C
$t$	= time, s
$\bar{x}$	= position vector
$r$	= radial direction
$z$	= axial direction
$\theta$	= azimuthal direction
$\alpha$	= ionization rate, 1/s
$\mu$	= mobility, m <sup>2</sup> /Vs
$\nu$	= collision frequency, 1/s
$\phi$	= electric potential, V
$\omega$	= perturbation frequency, rad/s
$\omega_c$	= cyclotron frequency, rad/s
$\omega_c \tau$	= Hall parameter

*Subscript*

$e$	= electron
$i$	= ion
$o$	= time average
$r$	= radial direction
$z$	= axial direction
$\theta$	= azimuthal direction

## I. Introduction

A Hall thruster is an electric propulsion device capable of providing continuous low thrust while maintaining high efficiency and propellant utilization.<sup>1</sup> In a typical Hall thruster, electrons travel from an external cathode to an anode at the base of an annular channel. Along their path, the electrons encounter a region of high resistivity due to an imposed radial magnetic field, and become trapped in an azimuthal  $E \times B$  Hall current. When neutral particles injected from the anode encounter this region of high electron density, electron impact ionization occurs. The newly born unmagnetized ions then accelerate out of the thruster due to the electrostatic potential maintained between the anode and cathode. While this process results in a high specific impulse device suitable for various low thrust applications, the physics behind Hall thruster operation is not well understood, particularly the mechanism which allows electrons to cross magnetic field lines.

Electron cross-field transport in Hall thrusters is experimentally observed to be higher than predicted by classical theory.<sup>2</sup> One possible mechanism producing anomalously high electron current is correlated azimuthal fluctuations in the electric field and plasma density within these devices. The most widely-used numerical model for predicting Hall thruster behavior is a radial-axial hybrid fluid-particle code. While this model is capable of producing many of the features observed within Hall-effect thrusters, such as the commonly observed "breathing mode" oscillations,<sup>3</sup> models of this type require empirical fitting parameters to accurately predict electron cross-field mobility. Since radial-axial hybrid models assume axisymmetric plasma properties, they are incapable of capturing the enhanced transport that results from azimuthal fluctuations. However, while these models lack resolution in the Hall direction, they generate a wide spectrum of frequencies and wavelengths corresponding to axial waves.<sup>4</sup> Although the relative phase of density and velocity fluctuations in the axial direction does not produce anomalous transport, these axial waves may couple into tilted axial-azimuthal waves which are capable of explaining the observed electron mobility.

This work will use a small-amplitude linear perturbation analysis to model the coupling of the axial waves generated by the radial-axial hybrid simulation into tilted axial-azimuthal waves. Despite the distribution of

simulated power in the hybrid Hall thruster model over a variety of wavelengths and frequencies, the analysis will be simplified by considering only the dominant frequency at a variety of wavelengths. The computed spatially-varying electron cross field transport within the interior of the Hall thruster channel caused by the inferred axial-azimuthal waves will be presented. Despite using a linear analysis to predict behavior in the non-linear saturation regime, the computational results will demonstrate that correlated fluctuations are capable of enhancing electron transport in Hall thrusters. Additionally, results of the linear analysis suggest that the transport barrier experimentally observed near the thruster exit may be due to a transition from transport-enhancing azimuthal waves to non-enhancing axial waves.

## II. Numerical Models

### A. Hybrid Hall Thruster Model

The numerical simulation used to calculate axial wave properties is a radial-axial hybrid fluid particle-in-cell (PIC) model<sup>5,6</sup> based on work by Fife.<sup>7</sup> The model employs a quasi-one-dimensional fluid treatment of electrons and a three-dimensional PIC treatment of the heavy species, Xe and Xe<sup>+</sup>. The two solutions are coupled assuming space-charge neutrality.

The computational geometry used in the simulation corresponds to the laboratory discharge referred to here as the Stanford Hall thruster.<sup>8</sup> The annular channel is approximately 8 cm in length and 1.2 cm in width. The computational grid, which includes a two-dimensional slice of the channel and near field region, is shown in Fig. 1. The insulating channel walls are made of alumina. A mass flow rate of 2 mg/s is implemented in the model to match experimental conditions. Measurements of the magnetic strength in the radial and axial directions along the channel centerline are used to impose a constant external magnetic field. A discharge voltage of 200 V is considered in the results presented here.

The electron fluid is governed by a continuity equation, momentum equations parallel and perpendicular to magnetic field lines, a one-dimensional electron energy equation, and a current continuity equation. Perpendicular to magnetic contours, an experimentally-based electron cross field mobility<sup>9</sup> is imposed in order to calculate the electron cross field velocity and thermal diffusivity. The electron mobility along magnetic field lines is assumed to be infinite resulting in isothermal magnetic field contours. Therefore, along field lines, the electric force is balanced by a pressure force resulting in a Boltzmann description of the electrons. The electron energy equation includes a Joule heating energy source term and ionization and wall damping energy sink terms. The wall damping treatment is similar to that of Barral *et al.*<sup>10</sup> However, while Barral calculates a separate electron temperature parallel to magnetic contours in order to determine the heat transfer to the wall, this model lowers the effective temperature at the wall to account for anisotropy and the non-Maxwellian nature of the electron velocity distribution function. The effective temperature used to compute wall energy loss producing the best agreement with experiment was found to be 40% of the perpendicular temperature computed from the 1D energy equation.

The motion of the heavy species, Xe and Xe<sup>+</sup>, is solved in three dimensions using cylindrical coordinates. Neutral particles are injected at the anode and scatter off channel walls assuming a one-way Maxwellian flux distribution. Ions which impact channel walls are neutralized before being re-emitted into the channel. Ionization<sup>11-14</sup> and charge exchange collisions<sup>15</sup> take place everywhere inside the computational domain based on local plasma properties. Neutral particles are injected from the computational boundaries in the near-field region in order to simulate a back pressure of 0.05 mTorr.

For computational manageability, macroparticles are used to represent large groups of neutrals and ions rather than simulating individual particles. Since neutral and ion densities differ by orders of magnitude over the length of the domain,

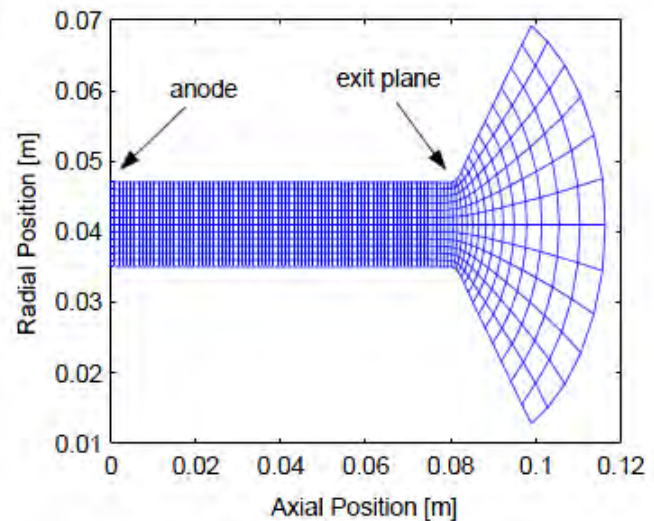


Figure 1. Computational grid of the Stanford Hall thruster radial-axial simulation.

the size of the superparticles vary with both space and species. The simulation is initialized with approximately 500,000 macroparticles of each heavy particle species. The ion and neutral timestep is 25 ns, while the electron timestep is 0.1 ns. The simulation completes 625  $\mu$ s in approximately one day on a 3.8 GHz Pentium 4 processor.

## B. Linearized Axial-Azimuthal Wave Model

As shown by Fernandez *et al.*, the axial waves generated by a radial-axial hybrid Hall thruster simulation can be understood using a simple linearized perturbation analysis.<sup>4</sup> However, due to the relative phase of the density and velocity fluctuations, the axial waves predicted by the linear analysis cannot be responsible for the observed anomalous electron cross field transport. Also, laboratory measurements may suggest that these waves do not exist in reality. While it is possible that the physics included in the radial-axial simulation are insufficient to describe experimental trends, another explanation is that the power produced in these axial waves is dissipated through wave coupling. Experimentally, physical grooves in the ceramic channel are found to develop at the exit plane of laboratory Hall thrusters after many hours of operation, suggesting the presence of standing waves. Therefore, in the analysis presented here, it is assumed that the axial waves generated by the radial-axial simulation couple symmetrically into two counter-propagating tilted waves with half the frequency and half the axial wavenumber, as shown in Fig. 2. Using a similar linear analysis as described in Ref. 4, a two-dimensional linearized dispersion relation can be derived in order to compute the azimuthal components of wavenumber consistent with the driving axial wave.

In this analysis, a fluid model is used to describe the electrons and ions, and a local assumption is enforced which neglects spatial non-uniformity of steady state properties. Small amplitude perturbations are assumed in order to linearize the continuity and momentum equations for the electrons and ions. All densities,  $n$ , and velocities,  $U$ , as well as the electric potential,  $\phi$ , are assumed to be composed of a steady state component,  $f_o$ , and a fluctuating component,  $\tilde{f} \exp(i(\vec{k} \cdot \vec{x} - \omega t))$ , as shown below.

$$f = f_o + \tilde{f} \exp(i(\vec{k} \cdot \vec{x} - \omega t)) \quad (1)$$

In this equation,  $\vec{k}$  is the wavevector and  $\omega$  is the frequency of the perturbation. Note that the fluctuation amplitude,  $\tilde{f}$ , may be complex in order to account for differences in phase.  $\vec{x}$  represents an arbitrary position vector such that:

$$\vec{k} \cdot \vec{x} = k_z z + k_\theta \theta \quad (2)$$

Despite the cylindrical nature of the problem, the coordinates  $z$ ,  $\theta$ , and  $r$  are treated as Cartesian. Note that  $k_r$  is assumed to be zero.

In the electron momentum equations, inertia terms are retained and a classical description based on electron-neutral collisions is used to describe the electron cross field mobility. Due to the predominantly axial steady state electric field, the steady state ion velocity is assumed to be purely axial. However, the small-amplitude fluctuating component of ion velocity will retain contributions in both the axial and azimuthal directions. Rather than incorporating a linearized version of the electron energy equation, the electron temperature is assumed not to exhibit oscillatory behavior. Lastly, the system of equations is closed assuming space-charge neutrality.

The system of equations to be solved is as follows:

### 1. Electron Continuity Equation

$$\frac{\partial n_e}{\partial t} + \frac{\partial(n_e U_{ez})}{\partial z} + \frac{\partial(n_e U_{e\theta})}{\partial \theta} = \alpha n_e \quad (3)$$

### 2. Ion Continuity Equation

$$\frac{\partial n_i}{\partial t} + \frac{\partial(n_i U_{iz})}{\partial z} + \frac{\partial(n_i U_{i\theta})}{\partial \theta} = \alpha n_i \quad (4)$$

### 3. Electron Axial Momentum Equation

$$\frac{\partial U_{ez}}{\partial t} + U_{ez} \frac{\partial U_{ez}}{\partial z} + U_{e\theta} \frac{\partial U_{ez}}{\partial \theta} = -\frac{e}{m_e} \left( E_z + \frac{1}{en_e} \frac{\partial p_e}{\partial z} + U_{e\theta} B_r \right) - \nu_e U_{ez} \quad (5)$$

### 4. Electron Azimuthal Momentum Equation

$$\frac{\partial U_{e\theta}}{\partial t} + U_{ez} \frac{\partial U_{e\theta}}{\partial z} + U_{e\theta} \frac{\partial U_{e\theta}}{\partial \theta} = -\frac{e}{m_e} \left( E_\theta + \frac{1}{en_e} \frac{\partial p_e}{\partial \theta} - U_{ez} B_r \right) - \nu_e U_{e\theta} \quad (6)$$

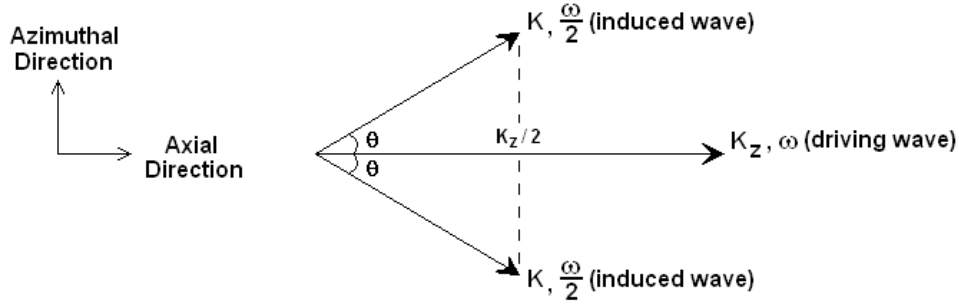


**Figure 2. Illustration of axial driving wave with given axial wavenumber and frequency coupling into two symmetric axial-azimuthal waves with half the axial wavenumber and frequency.**

5. *Ion Axial Momentum Equation*

$$\frac{\partial U_{iz}}{\partial t} + U_{iz} \frac{\partial U_{iz}}{\partial z} = \frac{e}{m_i} E_z - \alpha U_{iz} \quad (7)$$

6. *Ion Azimuthal Momentum Equation*

$$\frac{\partial U_{i\theta}}{\partial t} + U_{iz} \frac{\partial U_{i\theta}}{\partial z} = \frac{e}{m_i} E_\theta - \alpha U_{i\theta} \quad (8)$$

7. *Equation of Quasineutrality*

$$n_e = n_i \quad (9)$$

8. *Equation for an Electrostatic Field*

$$\vec{E} = -\nabla \phi \quad (10)$$

9. *Equation for Electron Pressure*

$$p_e = n_e k_b T_e \quad (11)$$

A detailed description of the solution of this system of equations through substitution of quantities of the form given by Eq. (1) is provided in Chapter 8 of Ref. 6. The linear analysis provides equations for the fluctuation amplitudes in terms of steady state quantities and wave properties. A summary of the resulting equations is given below:

1. *Electron Density Fluctuation Amplitude*

$$\tilde{n}_e = n_{e,o} \frac{\frac{-e}{m_e} \tilde{\phi}}{\frac{(\omega - \vec{k} \cdot \vec{U}_{e,o} + i\nu_e)^2 - \omega_{ce}^2}{k^2} \left( \frac{\omega - \vec{k} \cdot \vec{U}_{e,o} - i\alpha}{\omega - \vec{k} \cdot \vec{U}_{e,o} + i\nu_e} \right) - \frac{k_b T_e}{m_e}} \quad (12)$$

2. *Ion Density Fluctuation Amplitude*

$$\tilde{n}_i = n_{i,o} \frac{e}{m_i} \frac{k^2 \tilde{\phi}}{(\omega - k_z U_{iz,o})^2 + \alpha^2} \quad (13)$$

3. *Axial Electron Velocity Fluctuation Amplitude*

$$\tilde{U}_{ez} = \frac{\frac{-e}{m_e} \tilde{\phi} + \frac{k_b T_e}{m_e n_{e,o}} \tilde{n}_e}{(\omega - \vec{k} \cdot \vec{U}_{e,o} + i\nu_e)^2 - \omega_{ce}^2} \left( (\omega - \vec{k} \cdot \vec{U}_{e,o} + i\nu_e) k_z + i\omega_{ce} k_\theta \right) \quad (14)$$

#### 4. Azimuthal Electron Velocity Fluctuation Amplitude

$$\tilde{U}_{e\theta} = \frac{\frac{-e}{m_e} \tilde{\phi} + \frac{k_b T_e}{m_e n_{e,o}} \tilde{n}_e}{\left(\omega - \vec{k} \cdot \vec{U}_{e,o} + i\nu_e\right)^2 - \omega_{ce}^2} \left(-i\omega_{ce} k_z + \left(\omega - \vec{k} \cdot \vec{U}_{e,o} + i\nu_e\right) k_\theta\right) \quad (15)$$

#### 5. Axial Ion Velocity Fluctuation Amplitude

$$\tilde{U}_{iz} = \frac{e}{m_i} \frac{k_z \tilde{\phi}}{\left(\omega - k_z U_{iz,o} + i\alpha\right)} \quad (16)$$

#### 6. Azimuthal Ion Velocity Fluctuation Amplitude

$$\tilde{U}_{i\theta} = \frac{e}{m_i} \frac{k_\theta \tilde{\phi}}{\left(\omega - k_z U_{iz,o} + i\alpha\right)} \quad (17)$$

In the above equations, the cyclotron frequency is defined as:

$$\omega_c = \frac{qB}{m} \quad (18)$$

Once the fluctuation amplitudes have been found, a dispersion relation can be derived using the quasineutral assumption (Eq. (9)). Setting the electron density perturbation amplitude equal to the ion density perturbation amplitude yields:

$$-m_e \left( \left( \omega - \vec{k} \cdot \vec{U}_{e,o} + i\nu_e \right)^2 - \omega_{ce}^2 \right) \left( \frac{\omega - \vec{k} \cdot \vec{U}_{e,o} - i\alpha}{\omega - \vec{k} \cdot \vec{U}_{e,o} + i\nu_e} \right) - k_b T_e k^2 = m_i \left( \omega - k_z U_{iz,o} \right)^2 + \alpha^2 \quad (19)$$

This equation can be further simplified by defining the dot products as:

$$\vec{k} \cdot \vec{U}_{e,o} = kU_{e\parallel,o} \quad (20)$$

$$\vec{k} \cdot \vec{U}_{i,o} = k_z U_{iz,o} = kU_{i\parallel,o} \quad (21)$$

where the components of velocity parallel to the wave traveling at angle  $\gamma$  with respect to the  $z$ -direction are given by:

$$U_{e\parallel,o} = U_{ez,o} \cos \gamma + U_{e\theta,o} \sin \gamma \quad (22)$$

$$U_{i\parallel,o} = U_{iz,o} \cos \gamma \quad (23)$$

Using these substitutions and expanding Eq. (18) in terms of the angular frequency yields the following simplified dispersion relation:

$$C_3 \omega^3 + C_2 \omega^2 + C_1 \omega + C_0 = 0 \quad (24)$$

where:

$$C_3 = m_e + m_i \quad (25)$$

$$C_2 = -(2m_e + m_i) (kU_{e\parallel,o} - i\nu_e) - m_e (kU_{e\parallel,o} + i\alpha) - 2m_i kU_{i\parallel,o} \quad (26)$$

$$C_1 = m_e \left( (kU_{e\parallel,o} - i\nu_e)^2 - \omega_{ce}^2 \right) - k_b T_e k^2 + m_i \left( k^2 U_{i\parallel,o}^2 - \alpha^2 \right) \dots \quad (27)$$

$$\dots + 2m_i (kU_{e\parallel,o} - i\nu_e) kU_{i\parallel,o} + 2m_e (kU_{e\parallel,o} - i\nu_e) (kU_{e\parallel,o} + i\alpha) \\ C_0 = m_e (kU_{e\parallel,o} - i\nu_e)^2 (kU_{e\parallel,o} + i\alpha) + m_e (kU_{e\parallel,o} + i\alpha) \dots \quad (28) \\ \dots - m_i (kU_{e\parallel,o} - i\nu_e) k^2 U_{i\parallel,o}^2 + (kU_{e\parallel,o} - i\nu_e) k_b T_e k^2 + m_i (kU_{e\parallel,o} - i\nu_e) \alpha^2$$

Given the frequency of the perturbation and the axial component of wavenumber, azimuthal components of wavenumber can be found which are consistent with this dispersion relation.

### C. Linearized Fluctuation-Induced Mobility Model

In the radial-axial hybrid simulation, since azimuthal forces are neglected due to axisymmetry, the axial electron current density is related to the axial forces through the electron cross field mobility,  $\mu$ . Assuming that the magnetic field is primarily radial such that the perpendicular direction can be expressed by,  $z$ , the axial electron current density is given by:

$$J_{ez} = en_e \mu \left( E_z + \frac{1}{en_e} \frac{\partial p_e}{\partial z} \right) \quad (29)$$

Classically, the mobility is given by:

$$\mu_{classical} = \frac{e}{m_e} \frac{v_e}{(\omega_{ce}^2 + \nu_e^2)} \quad (30)$$

In most Hall thrusters, the electron cyclotron frequency,  $\omega_{ce}$ , dominates the electron collision frequency with heavy particles,  $\nu_e$ , in all regions of the channel such that the cross field mobility can be expressed as:

$$\mu = \frac{1}{(\omega_{ce}\tau)B} \quad (31)$$

where  $\omega_{ce}\tau$  is the dimensionless quantity called the Hall parameter. Neglecting azimuthal forces, the azimuthal electron current density is given by:

$$J_{e\theta} = en_e \frac{\left( E_z + \frac{1}{en_e} \frac{\partial p_e}{\partial z} \right)}{B_r} \quad (32)$$

Therefore, an effective Hall parameter can be defined in terms of the azimuthal and axial electron current densities as follows:

$$(\omega_{ce}\tau)_{eff} = \frac{J_{e\theta}}{J_{ez}} \quad (33)$$

In the radial axial hybrid simulation used to generate the axial waves on which this analysis is based, the effective Hall parameter was measured experimentally.<sup>2</sup> In many numerical models, the effective mobility is treated using adjustable fitting parameters which are optimized to produce agreement with experimental measurements. However, in order to simulate new thrusters or existing thrusters at operating conditions other than those for which experimental measurements have been made, the mechanism producing the anomalous transport should be understood. In this linear analysis, an effective Hall parameter is calculated using simulated plasma properties and inferred axial-azimuthal wave properties which are used to compute an anomalous axial electron current. The fluctuation-based Hall parameter is therefore determined using:

$$(\omega_{ce}\tau)_{eff} = \frac{(J_{e\theta})_{classical}}{(J_{ez})_{classical} - \frac{1}{2} e \text{Re}[\tilde{n}_e \tilde{U}_{ez}^*]} \quad (34)$$

In reality, the azimuthal current density will also consist of classical and fluctuating components. However, since the radial-axial hybrid simulation assumes uniformity in the azimuthal direction, the azimuthal current density is assumed in the numerical model to be given by Eq. (32) where all quantities are calculated based on time-averaged quantities. Also, in the above expression, the classical axial current density is given by Eq. (29) where in addition to using time-averaged quantities, the cross field mobility is based only on classical collisions between electrons and heavy particles.

### III. Results and Discussion

#### A. Simulated Axial Waves

By imposing the experimentally measured electron cross-field mobility profile, the radial-axial hybrid Hall thruster simulation exhibits various fluctuations in addition to the experimentally observed "breathing mode" oscillations. As an illustration, Fig. 3 demonstrates a simulated dispersion plot corresponding to a location near the exit plane of the thruster computed using a

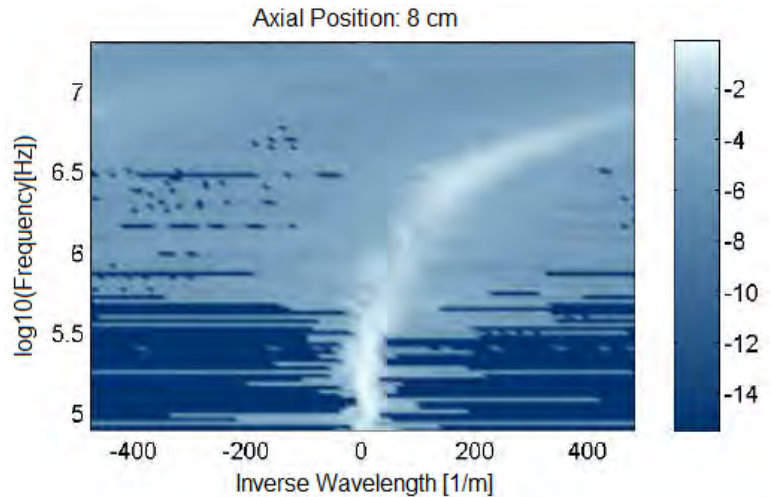


**Figure 3. Dispersion plot at an axial location of 8 cm along channel centerline, corresponding to the exit plane. The colorbar represents  $\log_{10}$  of total power in  $[V^2]$ .**

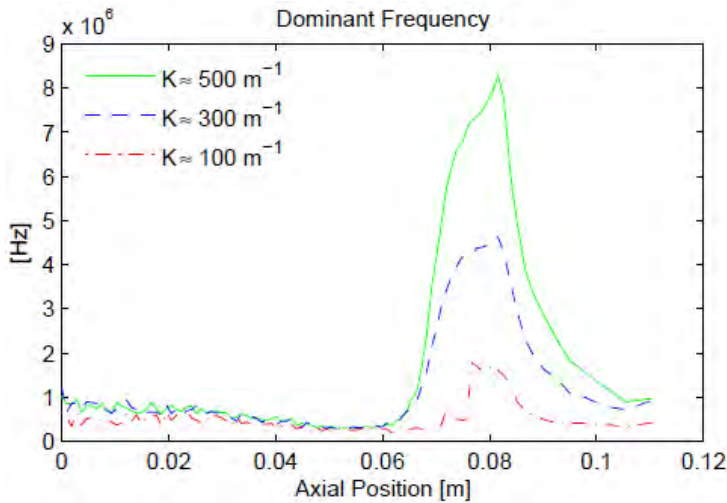


**Figure 4. Spatial dependence of simulated dominant frequency for three different axial wavenumbers.**

into the numerical model. In order to calculate the resulting transport due to wave-coupling, a more thorough analysis would account for the wide range of excited frequencies and wavenumbers. However, in this analysis, only a dominant frequency and wavenumber are considered. In order to evaluate the influence of different wavelength oscillations, three representative wavenumbers have been chosen for examination: 100, 300, and 500  $m^{-1}$ . Figure 4 shows the dominant frequency as a function of axial location along the centerline for each of these three axial wavenumbers. The dominant frequency was found to vary between  $\sim 500$  kHz and 8 MHz.

### B. Predicted Axial-Azimuthal Wave Coupling

Using the axial wave properties predicted by the radial-axial hybrid simulation, as shown in Fig. 4, the properties of the corresponding axial-azimuthal waves can be computed. As discussed in Section IIB, the axial driving wave is assumed to couple symmetrically into two counter-propagating axial-azimuthal waves. Therefore, each generated wave is assumed to have half the frequency and half the axial wavenumber as the

wavelet analysis of the simulated, time-dependent, spatially-varying plasma potential. Due to both the transient and spatially varying nature of the plasma properties, a Morlet wavelet analysis<sup>16</sup> was selected as a means to capture both the time-dependent frequency response, as well as reduce both noise and edge effects.

As shown Fig. 3, the simulated power is spread over a wide-range of frequencies and wavenumbers. The dominant frequency is found to increase as a function of increasing wavenumber, or decreasing wavelength. As previously mentioned, Fernandez *et al.*<sup>4</sup> has shown that the relationship between wavenumber and frequency exhibited by the hybrid model can be replicated through a linear analysis of the equations input

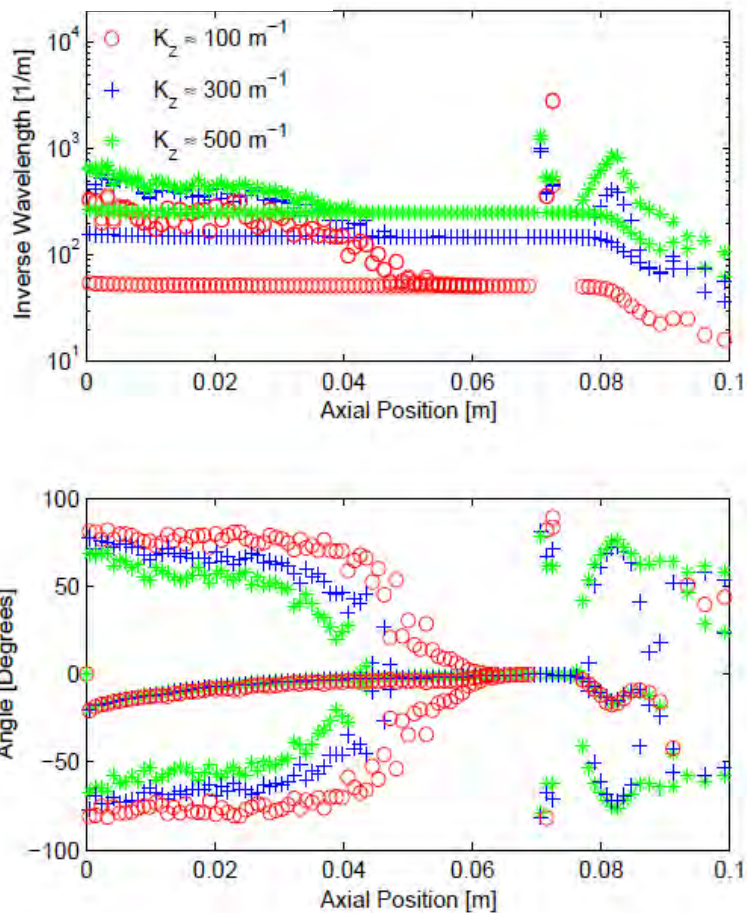


**Figure 5. Illustration of axial driving wave with given axial wavenumber and frequency coupling into two symmetric axial-azimuthal waves with half the axial wavenumber and frequency.**

simulated axial driving wave. Using these frequencies and wavenumbers at each location, along with time-averaged properties computed by the simulation, the fluctuation amplitudes and the azimuthal components of the wavenumbers can be computed through solution of the dispersion relation as given by Eqs. (24)-(28).

Figure 5 illustrates the computed magnitude and angle of propagation for the tilted waves for each of the three driving wave axial wavenumbers. Note that more than one magnitude and angle is possible at each location indicating that more than one solution exists to the dispersion relation which is consistent with the prescribed frequency and axial wavenumber. As shown in the upper plot of Fig. 5, the inverse wavelength of the tilted wave is found to vary between 50 and 700  $\text{m}^{-1}$  which corresponds to wavelengths between 1.5 mm and 2 cm. The lower plot of Fig. 5 shows that in addition to the predominantly axial root near zero degrees, there are two counter-propagating solutions, as expected, with propagation angles approaching  $\pm 90$  degrees near the anode corresponding to azimuthal waves which become more axial toward the exit plane at 8 cm. The smaller wavenumber case, corresponding to the largest considered driving wavelength of 1 cm, remains more strongly azimuthal for a greater region of the channel.

### C. Computed Mobility

Using the wave properties predicted in the previous section, combined with the steady state values calculated by the radial-axial hybrid model, an effective electron cross field Hall parameter can be computed from Eq. (34). In addition to the classical contribution to axial current based on time-averaged values, the computed Hall parameter is also based on correlated fluctuations between the electron density, given by Eq. (12), and the axial electron velocity, given by Eq. (14). The one remaining unknown parameter necessary in order to calculate a mobility profile is the power in the fluctuation related to the fluctuation amplitude of the potential,  $\tilde{\phi}$ . The fluctuation amplitude predicted by the wavelet analysis, represented by the solid black curve in Fig. 5, is insufficient to explain the anomalous electron transport observed in a Hall thruster. However, the wavelet-based potential fluctuation amplitude is calculated based on one narrow band in frequency and wavenumber. As illustrated by Fig. 3, power is distributed over a wide spectrum of frequencies and wavenumbers which have been neglected in this analysis. Therefore, in order to estimate the possible effect of including too little power, a potential fluctuation amplitude has been computed using a saturation model. This model, which defines the upper limit of the power contained in the wave, computes the potential fluctuation amplitude necessary such that the electron density perturbation amplitude,  $\tilde{n}_e$ , is equal to the steady state value,  $n_{e,0}$ , in Eq. (12). For comparison, the total power in three different frequency bands

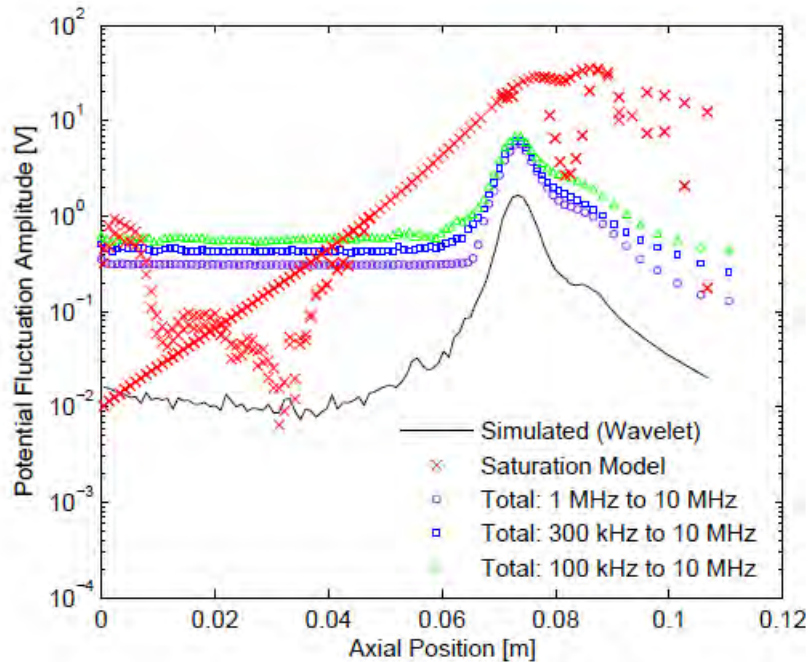


**Figure 6. Comparison of potential fluctuation amplitude computed using saturation model and wavelet analysis with total fluctuation amplitude in various frequency bands.**

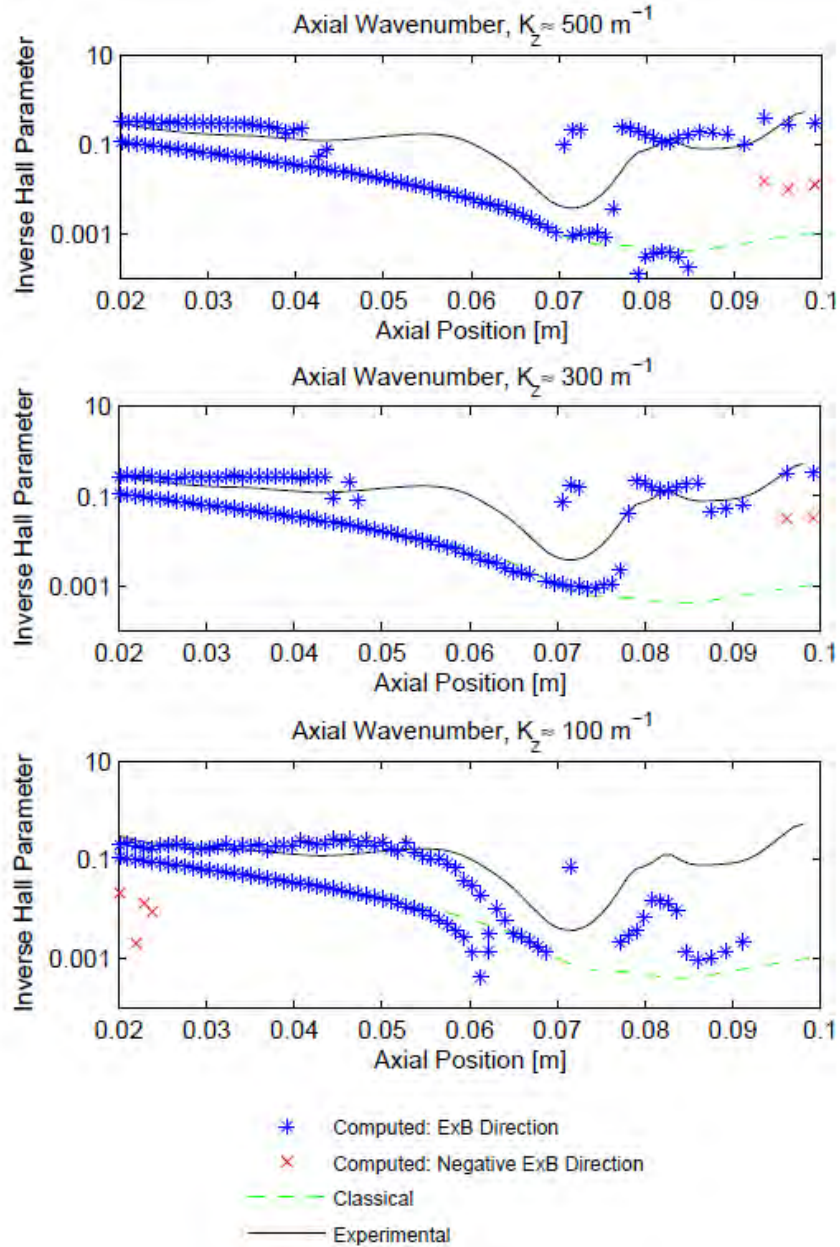


**Figure 7. Computed inverse Hall parameter using linear perturbation model assuming axial-azimuthal waves coupled to simulated axial waves. Saturation potential fluctuation is used rather than simulated value.**

computed from the simulation results is shown as well. Note that in the upstream region of the channel, the total simulated power is more than enough to saturate the wave. Downstream, the simulated variation in potential is not large enough to result in perturbation amplitudes on the order of the steady state electron density.

As an upper limit, the saturated potential amplitude has been used to compute electron transport from Eq. (34). The computed inverse Hall parameter is compared with the experimentally measured inverse Hall parameter in Fig. 7. The results indicate that one root of the solution corresponds to classical transport, while a second root results in anomalous transport upstream near the anode. The region of anomalous transport extends farther into the channel for smaller wavenumbers (larger wavelengths). While the model does predict a small region near 7 cm (approximately 1 cm upstream of the exit plane) where the transport is also anomalously high, in general, transport is seen to reduce near the exit place in the region where a transport barrier is experimentally found to exist. In the linearized model,

the region of reduced mobility is found to correspond to a transition from azimuthal to axial waves. Note that the best agreement occurs for the largest considered driving wavelength of 1 cm ( $100 \text{ m}^{-1}$ ). Although fluctuation magnitudes increase near the exit plane, the relative phase of the density and velocity perturbations result in less overall transport, reproducing experimentally observed trends.

#### IV. Summary

A linearized perturbation analysis has been performed to examine the possibility of wave coupling between the axial waves generated by a radial-axial hybrid Hall thruster model and axial-azimuthal waves which may be responsible for observed anomalous transport. The predicted tilted waves have frequencies on the order of several hundred kilohertz near the anode to a few megahertz near the exit plane. The wavelengths considered are on the order of millimeters to one centimeter. The angles of propagation of the tilted waves consistent with a dispersion relation derived based on a linearized analysis suggest that the tilted waves transition from almost purely azimuthal near the anode to nearly axial at the exit plane. Using saturation amplitudes for the potential fluctuations, the computed transport was found to qualitatively agree with experimental measurements. The predicted mobility is found to be anomalously high near anode and in the first half of the channel and transition to classical values in the second half of the channel near the exit plane. Based on the linear perturbation model, the reason for this transition is found to correspond to a transition from transport-enhancing azimuthal waves near the anode, where the density and velocity perturbations are in phase, to transport-suppressing axial waves near the exit plane, where the fluctuations are nearly 90 degrees out of phase.

#### Acknowledgments

This work was supported by the Air Force Office of Scientific Research. Stipend support for M.S. was provided by the Stanford Graduate Fellowship program.

#### References

- <sup>1</sup>Zhurin, V., Kaufman, H., and Robinson, R., "Physics of closed drift thrusters," *Plasma Sources Science and Technology*, Vol. 8, 1999.
- <sup>2</sup>Meezan, N., Hargus, W., and Cappelli, M., "Anomalous electron mobility in a coaxial Hall plasma discharge," *Physical Review E*, Vol. 63, No. 026420, 2001.
- <sup>3</sup>Boeuf, J., and Garrigues, L., "Low frequency oscillations in a stationary plasma thruster," *Journal of Applied Physics*, Vol. 84, pp. 3541, 1998.
- <sup>4</sup>Fernandez, E., Scharfe, M., Thomas, C. Gascon, N. and Cappelli, M., "Growth of resistive instabilities in ExB plasma discharge simulations," *Physics of Plasmas*, Vol. 25, No. 012102, 2008.
- <sup>5</sup>Fernandez, E. and Cappelli, M., "2D simulations of Hall thrusters," *CTR Annual Research Briefs*, pp. 81, 1998.
- <sup>6</sup>Scharfe, M., "Electron cross field transport modeling in radial-axial hybrid Hall thruster simulations," *Ph.D. Thesis, Stanford University*, 2009.
- <sup>7</sup>Fife, J.M., "Nonlinear hybrid-PIC modeling and electrostatic probe survey of Hall thrusters," *Ph.D. Thesis, Massachusetts Institute of Technology*, 1998.
- <sup>8</sup>Hargus, W., "Investigation of the plasma acceleration mechanism within a coaxial Hall thruster," *Ph.D. Thesis, Stanford University*, 2001.
- <sup>9</sup>Meezan, N., "Electron transport in a coaxial Hall discharge," *Ph.D. Thesis, Stanford University*, 2002.
- <sup>10</sup>Barral, S., Makowski, K., Peradzynski, Z. Gascon, N., and Dudeck, M., "Wall material effects in stationary plasma thrusters II: Near wall and inner-wall conductivity," *Physics of Plasmas*, Vol. 10, No. 10, 2003.
- <sup>11</sup>Rejoub, R., Lindsay, B., and Stebbings, R., "Determination of the absolute partial and total cross sections for electron-impact ionization of the rare gases," *Physical Review A*, Vol. 65, pp. 042713, 2002.
- <sup>12</sup>Nagy, P., Skutlartz, A. and Schmidt, V., "Absolute ionisation cross sections for electron impact in rare gases," *Journal of Physics B*, Vol. 14, pp. 1249, 1980.
- <sup>13</sup>Bell, E.W., Djuric, N., and Dunn, G., "Electron-impact ionization of  $\text{In}^+$  and  $\text{Xe}^+$ ," *Physical Review A*, Vol. 48, No. 6, pp. 4286, 1993.
- <sup>14</sup>Achenbach, C., Muller, A., Salzborn, E. and Becker, R., "Single ionization of multiply charged xenon ions by electron impact," *Journal of Physics B*, Vol. 17, pp. 1405, 1984.
- <sup>15</sup>Miller, J., Pullins, S., Levandier, D., Chiu, Y., and Dressler, R., "Xenon charge exchange cross sections for electrostatic thruster models," *Journal of Applied Physics*, Vol. 91, No. 3, pp. 984, 2002.
- <sup>16</sup>Thomas, C.A., "Anomalous electron transport in the Hall-effect thruster," *Ph.D. Thesis, Stanford University*, 2006.